Quantum study of inelastic processes in low-energy calcium–hydrogen collisions

A Belyaev, D Vlasov, A. O. Mitrushchenkov, N. Feautrier

Monthly Notices
of the
ROYAL ASTRONOMICAL SOCIETY

MNRAS **490,** 3384–3391 (2019)
Advance Access publication 2019 October 12

doi:10.1093/mnras/stz2763

Quantum study of inelastic processes in low-energy calcium–hydrogen collisions

A. K. Belyaev [1]★ D. V. Vlasov,[1,2] A. Mitrushchenkov[3] and N. Feautrier[4]

[1]*Department of Theoretical Physics and Astronomy, Herzen University, St Petersburg 191186, Russia*
[2]*T-Systems Rus, St. Petersburg 199034, Russia*
[3]*Laboratoire Modélisation et Simulation Multi Echelle, MSME UMR 8208, CNRS, UPEC, UPEM, Université Paris-Est, 5 Bd Descartes, Champs-sur-Marne, F-77454 Marne la Vallée, France*
[4]*LERMA, Observatoire de Paris, Sorbonne University, UPMC Univ. Paris 06, CNRS-UMR 8112, F-92195 Meudon, France*

Accepted 2019 September 26. in original form 2019 July 25

ABSTRACT

Cross-sections and rate coefficients for the partial inelastic processes in calcium–hydrogen collisions are calculated by means of the quantum reprojection method for nuclear dynamics based on the accurate *ab initio* electronic structure data. That is, the atomic data for the 110 inelastic processes of excitation, de-excitation, ion-pair formation, and mutual neutralization in Ca + H and $Ca^+ + H^-$ collisions are computed for all transitions between the 11 low-lying $CaH(^2\Sigma^+)$ molecular states including ionic one. The quantum chemical data are used in a hybrid diabatic representation, which is derived from the adiabatic representation. It is found that the largest rate coefficients correspond to the mutual neutralization processes. At the temperature 6000 K, the maximal rate is equal to 4.37×10^{-8} cm^3 s^{-1}. It is shown that the large-valued rates are determined by long-range ionic–covalent interactions with final binding energies from the optimal window, while moderate- and low-valued rates by both long- and short-range non-adiabatic regions with final energies outside of the optimal window.

Key words: atomic data – atomic processes – scattering – stars: abundances.

1 INTRODUCTION

Determining relative and absolute abundances of different chemical elements is of fundamental importance in astrophysics (see e.g. reviews Asplund 2005; Barklem 2016a and references therein). This can be done either by Local Thermodynamic Equilibrium (LTE) or more accurately by non-Local Thermodynamic Equilibrium (non-LTE) line formation modelling (Plaskett 1955; Steenbock & Holweger 1984; Lambert 1993; Asplund 2005; Barklem 2016a). While conventional LTE modelling does not require data on inelastic processes, non-LTE modelling does require such data, in particular, on radiative processes and on inelastic processes in collisions of heavy atomic particles (atoms, ions) and electrons or hydrogen (atoms, cations). It has been shown that data on inelastic processes in collisions with hydrogen give the main uncertainty in non-LTE modelling (see e.g. Asplund 2005; Barklem 2016a). Because of the lack of accurate quantum data, the so-called classical Drawin formula (Drawin 1968, 1969; Steenbock & Holweger 1984) has been used for determining heavy-particles collisional rate coefficients often with adjustable scaling factors. Later on it was recognized that the Drawin formula does not have a physical background and does not provide reliable data even with adjustable factors (Barklem et al. 2011). So, quantum data on inelastic collisions with hydrogen are highly desirable.

Reliable data can be obtained by means of a model approach or by a complete quantum study. The later is the most accurate, but full quantum approaches are still time consuming and have been applied only to a few systems involving collisions with hydrogen: Na + H and $Na^+ + H^-$ (Belyaev et al. 1999, 2010), Li + H and $Li^+ + H^-$ (Croft, Dickinson & Gadéa 1999a,b; Belyaev & Barklem 2003), $H^+ + H^-$ (Stenrup, Larson & Elander 2009), Mg + H, and $Mg^+ + H^-$ (Belyaev et al. 2012; Guitou et al. 2015). For this reason, this paper reports the results of the complete quantum treatment of inelastic processes in calcium–hydrogen collisions.

Calcium is of particular interest in astrophysics. It plays an important role in studies of stellar atmospheres, since calcium is an α-element and produced by supernovae. In wide range of stellar parameters, calcium is observed in the two ionization stages, Ca I and Ca II, and it is one of the best observable chemical elements in late-type stars (Mashonkina, Korn & Przybilla 2007; Mashonkina, Sitnova & Belyaev 2017; Sitnova, Mashonkina & Ryabchikova 2018). This opens a way to determine stellar atmosphere parameters and as well as calcium abundance by using both Ca I and Ca II lines. As the result, dependences of Ca I and Ca II lines formation on deviations from LTE modelling should be determined in non-LTE modelling.

★ E-mail: andrey.k.belyaev@gmail.com

Statistical equilibrium of Ca I and Ca II lines has been studied in the past (see e.g. Drake 1991; Idiart & Thevenin 2000; Mashonkina et al. 2007, 2017 and references therein). Several non-LTE calcium stellar spectra modellings have been performed as well (Idiart & Thevenin 2000; Christlieb et al. 2002; Frebel et al. 2005, 2015; Mashonkina et al. 2007; Norris et al. 2007; Caffau et al. 2011; Cohen et al. 2013; Mashonkina, Sitnova & Pakhomov 2016; Mashonkina et al. 2017; Sitnova et al. 2018). In these papers, except for Mashonkina et al. (2016, 2017) and Sitnova et al. (2018), rate coefficients for inelastic processes in calcium–hydrogen collisions were estimated by the classical Drawin formula. Since the Drawin formula is unreliable, the required rate coefficients for calcium–hydrogen collisions were evaluated later on by model quantum approaches. First, they were computed by Belyaev et al. (2016) by means of the asymptotic semi-empirical model (Belyaev 2013) for electronic structure followed by the multichannel Landau–Zener (LZ) model (Belyaev 1993; Yakovleva, Voronov & Belyaev 2016) for non-adiabatic nuclear dynamics. This approach picks up the dominant contribution coming from the long-range non-adiabatic regions created by the ionic–covalent interaction. Since the ground-state molecular ionic configuration has the $^2\Sigma^+$ molecular symmetry, the large-valued inelastic transition probabilities, cross-sections, and rate coefficients are determined by transitions within this symmetry. These rate coefficients for the processes in Ca + H and Ca^+ + H^- collisions were used for non-LTE modelling by Mashonkina et al. (2016), Mashonkina et al. (2017), and Sitnova et al. (2018). Later on the calcium–hydrogen collisional rate coefficients were calculated by Barklem (2016b) and Barklem (2017) by means of the asymptotic two-electron Linear Combinations of Atomic Orbitals (LCAO) approach for electronic structure followed by the same multichannel LZ model, that is, based on the long-range non-adiabatic ionic–covalent interactions. It has been shown that both approaches yield the rates roughly with the same accuracy on average, especially for processes with the largest rates that are in good agreement with quantum results, where available. Recently, the accurate *ab initio* CaH electronic structure calculations have been performed by Mitrushchenkov et al. (2017). The accurate adiabatic potentials and non-adiabatic couplings allow one not only to improve a long-range non-adiabatic nuclear dynamical treatment by calculating more accurate parameters of non-adiabatic regions, but also include short-range non-adiabatic regions into consideration. This has been accomplished by Belyaev et al. (2017) by means of the probability current method (Belyaev 2013), which takes into account all non-adiabatic regions, short and long range, based on the accurate potentials (Mitrushchenkov et al. 2017). Both features, more accurate non-adiabatic parameters and inclusion of short-range non-adiabatic regions, increase accuracy of the calculated rate coefficients. On the other hand, having the accurate CaH electronic structure known (Mitrushchenkov et al. 2017), one can study non-adiabatic nuclear dynamics by a complete quantum method and obtain the most accurate data on inelastic processes in Ca + H and Ca^+ + H^- collisions. This is performed in this work by means of the reprojection method (see Grosser, Menzel & Belyaev 1999; Belyaev et al. 2001; Belyaev 2010 for the method).

It is worth mentioning that an accurate non-LTE treatment requires information not only about the collisional processes in the CaH system, but also in the CaH^+ one, that is, in Ca^+ + H, Ca^{2+} + H^-, and Ca + H^+ collisions. These data are currently available from the recent calculations (Belyaev, Voronov & Gadéa 2018). The calculations are performed by means of the probability current method based on the accurate *ab initio* CaH^+ adiabatic potentials.

Table 1. CaH($j^2\Sigma^+$) molecular states taken into account in this study, the corresponding scattering channels, their asymptotic excitation energies with the respect to the ground-state level, the asymptotic binding energies, and the statistical probabilities $p_j^{\rm stat}$ for population of the molecular states. The state $j = 11$ is also marked by '*ion*' and corresponds to the ionic pair.

j	Scattering channels	Asymptotic energies (eV)	Binding energies (eV)	$p_j^{\rm stat}$
1	$Ca(4s^2\,^1S) + H(1s\,^2S)$	0.0	−6.113	1.0
2	$Ca(4s4p\,^3P) + H(1s\,^2S)$	1.892	−4.221	0.11111
3	$Ca(3d4s\,^3D) + H(1s\,^2S)$	2.524	−3.589	0.06667
4	$Ca(3d4s\,^1D) + H(1s\,^2S)$	2.709	−3.404	0.2
5	$Ca(4s4p\,^1P) + H(1s\,^2S)$	2.933	−3.180	0.33333
6	$Ca(4s5s\,^3S) + H(1s\,^2S)$	3.910	−2.203	0.33333
7	$Ca(4s5s\,^1S) + H(1s\,^2S)$	4.131	−1.982	1.0
8	$Ca(3d4p\,^3F) + H(1s\,^2S)$	4.442	−1.671	0.04762
9	$Ca(4s5p\,^3P) + H(1s\,^2S)$	4.534	−1.579	0.11111
10	$Ca(4s5p\,^1P) + H(1s\,^2S)$	4.554	−1.559	0.33333
11(*ion*)	$Ca^+(4s^2S) + H^-(1s^2\,^1S)$	5.363	−0.750	1.0

2 CALCIUM–HYDROGEN LOW-ENERGY COLLISIONS

2.1 Quantum-chemical data in hybrid diabatic representation

Mitrushchenkov et al. (2017) calculated *ab initio* CaH adiabatic potentials for the following molecular symmetries: $^2\Sigma^+$, $^2\Sigma^-$, $^2\Pi$, $^2\Delta$, and $^2\Phi$. It has been shown by the model studies of calcium–hydrogen collisional processes (see e.g. Belyaev et al. 2016) that the dominant non-adiabatic transitions occur in the CaH($^2\Sigma^+$) molecular symmetry. For this reason only this symmetry is included into the present full quantum study of the inelastic processes in calcium–hydrogen collisions. The accurate *ab initio* electronic structure calculations (Mitrushchenkov et al. 2017) comprise the 11 low-lying CaH($^2\Sigma^+$) molecular states, and they are all included into the present CaH nuclear dynamic treatment. They contain 10 covalent Ca + H states and one ionic Ca^+ + H^- state ($j = 11$). These molecular states and the corresponding scattering channels are listed in Table 1. The higher lying molecular states with potentials located above the 10th adiabatic potential are not taken into consideration since the system passes the corresponding non-adiabatic regions practically diabatically. Therefore, the ionic potential is extended by the asymptotic Coulomb behaviour for the energies above the asymptotic 10th potential.

The calculated CaH($^2\Sigma^+$) adiabatic potential energies, the non-adiabatic radial coupling derivative matrix elements $\langle\phi_j|\partial/\partial R|\phi_k\rangle$, R being the internuclear distance, as well as the discussion of the calculated data are presented in the paper of Mitrushchenkov et al. (2017). $\{|\phi_j\rangle\}$ are the adiabatic electronic molecular functions. In particular, it was found that some of the derivative coupling matrix elements remain non-zero in the asymptotic region, $R \to \infty$, when the electronic coordinates are measured from the centre of nuclear mass. It is known, that this is the fundamental feature of the Born–Oppenheimer approach. It makes a challenge for the Born–Oppenheimer treatment, but the reprojection method (Grosser et al. 1999; Belyaev et al. 2001; Belyaev 2010) solves this challenge.

In general, coupled channel equations can be solved numerically in an adiabatic representation. However, in practice one meets severe difficulties in numerically integrating coupled channel equations in presence of narrow avoided crossings in an adiabatic representation. On the other hand, one also meets problems in making transformations from an adiabatic to a diabatic representation, if there are non-zero asymptotic non-adiabatic couplings. Moreover,

Table 2. δ-like non-adiabatic matrix elements $D^{\phi}_{jk}(R) \equiv \langle \phi_j \,|\partial/\partial R|\, \phi_k \rangle$ (in atomic units = au), their positions, heights, half-widths from the CaH($^2\Sigma^+$) quantum-chemical data in the adiabatic representation, R_0 being a centre of a corresponding non-adiabatic region.

$\langle \phi_j \left\| \frac{\partial}{\partial R} \right\| \phi_k \rangle$	R_0 (au)	$\langle \phi_j \left\| \frac{\partial}{\partial R} \right\| \phi_k \rangle \Big\|_{R=R_0}$ (au)	Half-width (au)
$\langle \phi_8 \left\| \frac{\partial}{\partial R} \right\| \phi_9 \rangle$	29.6340322	1.227×10^4	8.1495×10^{-5}
$\langle \phi_8 \left\| \frac{\partial}{\partial R} \right\| \phi_9 \rangle$	9.7788768	46.18	2.1655×10^{-2}
$\langle \phi_8 \left\| \frac{\partial}{\partial R} \right\| \phi_9 \rangle$	6.2800250	18.92	5.286×10^{-2}
$\langle \phi_4 \left\| \frac{\partial}{\partial R} \right\| \phi_5 \rangle$	5.2377523	−32.85	3.044×10^{-2}
$\langle \phi_3 \left\| \frac{\partial}{\partial R} \right\| \phi_4 \rangle$	3.5693	22.24	4.4969×10^{-2}
$\langle \phi_{10} \left\| \frac{\partial}{\partial R} \right\| \phi_{11} \rangle$	4.4895217	96.87	1.032×10^{-2}

diabatic potentials not necessary cross each other, and these non-crossing potentials do not help to solve a problem of narrow non-adiabatic regions. The present *ab initio* CaH($^2\Sigma^+$) potentials exhibit several narrow non-adiabatic regions with δ-like non-adiabatic couplings, they are collected in Table 2. In order to solve these problems, Vlasov, Rodionov & Belyaev (2018) proposed to make transformations to a hybrid representation only in narrow non-adiabatic regions, the transformations which guarantee crossing diabatic potentials instead of avoided crossings. In addition, a hybrid representation can be constructed even in presence of non-zero asymptotic couplings.

The idea of the hybrid representation is to construct a transformation from a two-state narrow avoided crossing in the adiabatic representation to a two-state diabatic representation with crossing potentials based on a model, in particular, on the LZ model; within the LZ model the non-adiabatic coupling has the Lorentzian form. Other narrow non-adiabatic regions and molecular states are transformed separately one-by-one where necessary keeping residual non-adiabatic couplings. Finally, one has smooth non-zero off-diagonal and diagonal matrix elements and smooth residual couplings instead of narrow avoided crossings (and sharp potentials and couplings) in the coupled channel equations for a non-adiabatic nuclear dynamical treatment. In practice, one treats a two-state narrow avoided crossing separately from other states and other non-adiabatic regions, then picks out a model non-adiabatic coupling $D^{\rm model}_{jk}(R)$ from the original non-adiabatic coupling $\langle \phi_j \,|\partial/\partial R|\, \phi_k \rangle \equiv D^{\phi}_{jk}(R)$ calculated in the adiabatic representation

$$D^{\phi}_{jk}(R) = D^{\rm model}_{jk}(R) + D^{\rm res}_{jk}(R)\,, \tag{1}$$

where $D^{\rm res}_{jk}(R)$ is a residual derivative coupling. The adiabatic molecular functions $\{|\phi_j\rangle\}$ are related to a hybrid molecular basis $\{|\chi_k\rangle\}$ by a unitary transformation matrix $\mathbf{C}$

$$|\chi\rangle = \mathbf{C}\,|\phi\rangle\ . \tag{2}$$

Within the LZ model, the non-adiabatic matrix element for two adjacent adiabatic states is determined by the Lorentzian formula

$$D^{\rm model}_{jk}(R) = D^{\rm LZ}_{jk}(R) = \frac{\tau}{(R-R_0)^2 + 4\tau^2}\,, \tag{3a}$$

$$\tau = \frac{H_{jk}}{\left|{\rm d}H_{jj}/{\rm d}R - {\rm d}H_{kk}/{\rm d}R\right|}\,, \tag{3b}$$

where the Hamiltonian matrix elements H_{jk}, H_{jj}, and H_{kk} are defined for two adjacent molecular states j and k in a diabatic representation χ. The internuclear distance R_0 is defined as the separation corresponding to a minimum of an adiabatic potential splitting. One can see that the height of the coupling is equal to $1/4\tau$, and this defines the non-adiabatic coupling $D^{\rm LZ}_{jk}(R)$ within the LZ model in the non-adiabatic region (having R_0 known), see equation (3a).

One may choose different matrices $\mathbf{C}$ depending on desired properties of a hybrid basis $\{|\chi_k\rangle\}$. One of the possibilities is to use not the whole derivative coupling D^{ϕ}_{jk} for determining a transformation matrix $\mathbf{C}$, but only a part of a coupling, namely, a model coupling $D^{\rm model}_{jk}$, e.g. the LZ coupling $D^{\rm LZ}_{jk}$, equation (3a). In this case, the transformation coefficient elements of a matrix $\mathbf{C}$, equation (2), obey the following system of first-order differential equations

$$\frac{\rm d}{{\rm d}R}\mathbf{C} = \mathbf{C}\,\mathbf{D}^{\rm LZ}\,, \tag{4}$$

where the matrix elements of the derivative couplings are the model couplings $D^{\rm LZ}_{jk}(R)$, equation (3a), which can deviate from the couplings obtained in the adiabatic representation, see equation (1). Equation (4) is solved separately in narrow non-adiabatic regions with the asymptotic boundary conditions in the form of the unit matrix $\mathbf{C} = \mathbf{I}$ at a distant internuclear distance. Note that in general, model derivative couplings $D^{\rm model}_{jk}(R)$ might deviate from the LZ coupling $D^{\rm LZ}_{jk}(R)$, see equation (3a).

Applying a hybrid diabatization one time (with a transformation matrix $\mathbf{C}_1$ in one narrow non-adiabatic region), one has the electronic Hamiltonian matrix $\mathbf{H}^{\chi}$ in desired forms with crossing potentials and a non-zero off-diagonal matrix element in one selected non-adiabatic region. In this desired hybrid representation, the first derivative coupling matrix $\mathbf{D}^{\chi}$ will be changed as well and presented by the residual couplings $\mathbf{D}^{\rm res}$. Applying consistently a hybrid diabatization N times (with transformation matrices $\mathbf{C}_1, \ldots, \mathbf{C}_N$) one-by-one in narrow non-adiabatic regions (N diabatization procedures in total), one finally has the electronic Hamiltonian matrix

$$\mathbf{H}^{\chi} = \left(\mathbf{C}_N^{+}\left(\ldots\left(\mathbf{C}_2^{+}\left(\mathbf{C}_1^{+}\mathbf{U}\mathbf{C}_1\right)\mathbf{C}_2\right)\ldots\right)\mathbf{C}_N\right)\,, \tag{5}$$

and the first derivative coupling matrix

$$\begin{aligned}\mathbf{D}^{\chi} &= \left(\mathbf{C}_N^{+}\left(\ldots\left(\mathbf{C}_2^{+}\left(\mathbf{C}_1^{+}\left(\mathbf{D}^{\phi} + \frac{d}{dR}\right)\mathbf{C}_1\right)\mathbf{C}_2\right)\ldots\right)\mathbf{C}_N\right)\\ &= \mathbf{D}^{\rm res}\,,\end{aligned} \tag{6}$$

$\mathbf{U}$ being the (diagonal) electronic Hamiltonian matrix in the adiabatic representation. $\mathbf{D}^{\rm res}$ is a matrix constructed from the residual couplings, obtained from equation (1) in each narrow non-adiabatic region. A similar equation can be written for the second-derivative matrix $\mathbf{D}^{(2)}_{\chi}$ in the hybrid representation (see Vlasov et al. 2018).

It is worth mentioning that usage of the Lorentzian function (3a) in equation (4) for calculations of transformation matrices $\mathbf{C}$ guarantees crossing diabatic potentials in each selected non-adiabatic region since an absolute value of the integral of the Lorentzian function over R is equal to $\pi/2$.

Thus, the hybrid diabatization can be applied to selected (narrow) non-adiabatic regions and it results in crossing diabatic potentials in these (narrow) regions with non-zero off-diagonal Hamiltonian matrix elements as well as with residual non-adiabatic (derivative) coupling matrix elements including non-zero couplings in the asymptotic region. The coupled channel equations include both the off-diagonal Hamiltonian matrix elements and the residual derivative matrix elements and this does not create a problem in numerical integration since there is no narrow avoided crossings in the quantum chemical data in the described hybrid representation.

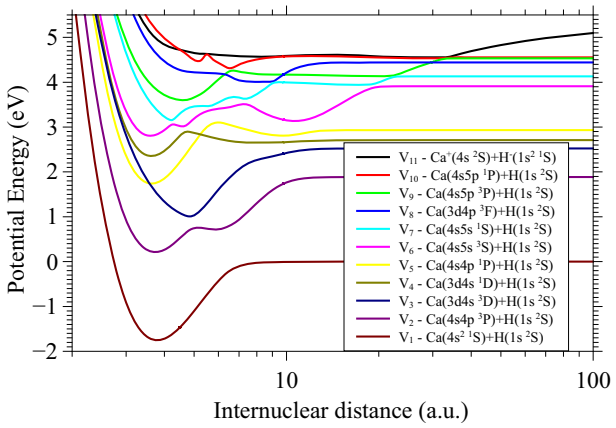

Figure 1. Diabatized potential energies of CaH($^2\Sigma^+$) in the hybrid representation as functions of the internuclear distance.

It is also worth mentioning some other approaches to transform to a diabatic representation in a selected non-adiabatic regions (see Mitrushenkov et al. 2000; Roos, Orel & Larson 2009a; Roos et al. 2009b; Voorhis et al. 2010; Zanchet et al. 2016). The main idea of these approaches is to minimize non-adiabatic matrix elements (Voorhis et al. 2010), which is implemented by different methods (Mitrushenkov et al. 2000; Roos et al. 2009a,b; Zanchet et al. 2016), typically by varying transformation matrix parameters. In particular, Roos et al. (2009a, b) and Zanchet et al. (2016) have used a sequence of partial transformation matrices in addition to varying adjustable parameters. The present approach deviates from the previous ones by making transformation to a hybrid representation in narrow regions and splitting non-adiabatic couplings into two parts. A particular implementation is based on the LZ type couplings (Landau 1932a,b; Zener 1932) and this guarantees crossing of selected diabatic potentials in each treated non-adiabatic region.

The collision system CaH has several narrow non-adiabatic regions with sharp peaks of the couplings $D^{\phi}_{jk}(R)$ as functions of the internuclear distance. They are collected in Table 2. These regions are problematic for numerical integration of the coupled channel equations and hence the subjects for application of the hybrid diabatization described above in order to modify the quantum chemical data into the hybrid representation.

The detailed description of the hybrid diabatization procedure can be found in the paper of Vlasov et al. (2018). It is worth mentioning the difference between this work and the work of Vlasov et al. (2018): the additional non-adiabatic region around $R_0 = 3.5693$ atomic units (atomic units = au) for the coupling $\langle\phi_3|\partial/\partial R|\phi_4\rangle$ is taken into account in this work and a 3×3 transformation matrix $\mathbf{C}$ is computed accounting for two regions simultaneously, around $R_0 = 5.2377523$ au for the matrix element $\langle\phi_4|\partial/\partial R|\phi_5\rangle$ and around $R_0 = 3.5693$ au for the coupling $\langle\phi_3|\partial/\partial R|\phi_4\rangle$. Thus, in the present case $N = 5$, though six narrow non-adiabatic regions has been diabatized.

The calculated CaH($^2\Sigma^+$) potentials obtained in the hybrid representation are shown in Fig. 1. Each plotted potential, which has been diabatized, has a crossing(s) with a neighbouring potential(s) in the vicinity of the internuclear distances listed in Table 2. Since the treated non-adiabatic regions are narrow, they are typically well separated, and hence, outside of these regions, the hybrid quantum chemical data coincide with the adiabatic data obtained in Mitrushchenkov et al. (2017).

2.2 Nuclear dynamical treatment

The present nuclear dynamical treatment of calcium–hydrogen collisions is performed by means of the quantum reprojection method (Grosser et al. 1999; Belyaev et al. 2001; Belyaev 2010), which is based on numerical integration of the coupled channel equations followed by calculations of the scattering matrix. This is done in the hybrid representation described above. In this representation, the coupled channel equations comprise both the off-diagonal electronic Hamiltonian matrix elements and the radial non-adiabatic couplings, and they all can induce non-adiabatic transitions. Moreover, the hybrid representation is applied to the narrow non-adiabatic regions only. Therefore, in the asymptotic region the hybrid representation coincides with the adiabatic one. This leads to the fact that the asymptotic radial non-adiabatic coupling matrix elements $\langle\chi_j|\partial/\partial R|\chi_k\rangle$ remain non-zero, since this is the fundamental feature of the Born–Oppenheimer approach. Having radial non-adiabatic couplings non-zero in the asymptotic region where the scattering matrix is calculated, one has to take these non-zero matrix elements into account. Within the formalism of the reprojection method (Grosser et al. 1999; Belyaev et al. 2001; Belyaev 2010), the scattering matrix calculations are performed in the adiabatic representation by means of construction of correct incoming and outgoing asymptotic wave functions, and non-zero radial non-adiabatic couplings are needed for this construction.

The coupled channel equations contain second derivative radial non-adiabatic couplings as well. The corresponding formulas for these couplings in the hybrid representation are derived in Vlasov et al. (2018). However, since the δ-like first derivative radial couplings are removed, the second derivative couplings get small and can be estimated from the first derivative residual couplings (Belyaev et al. 1999). Ultimately, they give small corrections only.

The final step is calculations of the partial cross-sections and rate coefficients for collision processes of interest. Since exothermic processes, mutual neutralization, and de-excitation at present, have no energy thresholds, it is more practical to compute partial cross-sections $\sigma_{if}(E)$ and rate coefficients $K_{if}(T)$ first for the exothermic processes $i \to f\,(E_i > E_f)$ by the following formulas

$$\sigma_{if}(E) = \frac{\pi\hbar^2 p_i^{\rm stat}}{2ME}\sum_{J=0}^{\infty} P_{if}(E,J)(2J+1)\,, \tag{7}$$

$$K_{if}(T) = \sqrt{\frac{8}{\pi M\,(k_{\rm B}T)^3}}\int_0^{\infty}\sigma_{if}(E)E\exp\left(-\frac{E}{k_{\rm B}T}\right)\mathrm{d}E\,, \tag{8}$$

where E is the collision energy, J the total angular momentum quantum number, M the reduced nuclear mass, $p_i^{\rm stat}$ the statistical probability of the initial channel i, $k_{\rm B}$ the Boltzmann constant, T a temperature. The cross-sections $\sigma_{fi}(E)$ and rate coefficients $K_{fi}(T)$ for the inverse processes $f \to i$, the endothermic excitation and ion-pair formation ones, can be then calculated from equations (7) and (8) by the detailed balance relations

$$\sigma_{fi}(E) = \left[\frac{p_f^{\rm stat}}{p_i^{\rm stat}}\frac{E-\Delta E_{if}}{E}\right]\sigma_{if}(E-\Delta E_{if})\,, \tag{9}$$

$$K_{fi}(T) = \left[\frac{p_f^{\rm stat}}{p_i^{\rm stat}}\exp\left(-\frac{\Delta E_{if}}{k_{\rm B}T}\right)\right]K_{if}(T)\,, \tag{10}$$

where $\Delta E_{if} = E_i - E_f$ is the energy defect between channels i and f.

Table 3. Rate coefficients in units $cm^3\ s^{-1}$ for temperature $T = 3000$ K.

	1	2	3	4	5	6	7	8	9	10	11
1	–	3.06e-15	1.12e-16	9.39e-19	7.19e-19	6.59e-20	2.71e-20	1.48e-20	6.28e-21	4.58e-21	4.25e-22
2	5.00e-13	–	3.14e-11	1.04e-13	6.05e-14	3.17e-15	1.20e-15	5.12e-16	1.78e-16	1.24e-16	8.60e-18
3	1.30e-13	2.21e-10	–	1.47e-12	4.60e-13	3.09e-14	1.33e-14	6.47e-15	1.69e-15	2.45e-15	3.72e-16
4	6.68e-15	4.54e-12	9.07e-12	–	9.49e-11	2.17e-12	4.64e-13	1.43e-13	5.97e-14	8.68e-14	1.09e-14
5	2.02e-14	1.04e-11	1.12e-11	3.75e-10	–	1.16e-11	2.72e-12	5.63e-13	1.89e-13	3.79e-13	7.56e-14
6	8.14e-14	2.40e-11	3.30e-11	3.77e-10	5.10e-10	–	9.44e-10	6.71e-11	1.19e-10	3.55e-10	6.62e-11
7	2.36e-13	6.38e-11	1.00e-10	5.67e-10	8.42e-10	6.64e-09	–	1.65e-10	9.50e-10	2.65e-09	4.42e-10
8	2.03e-14	4.31e-12	7.70e-12	2.77e-11	2.76e-11	7.48e-11	2.62e-11	–	4.42e-11	4.88e-11	6.44e-12
9	2.87e-14	4.97e-12	6.69e-12	3.83e-11	3.07e-11	4.39e-10	4.99e-10	1.47e-10	–	1.82e-09	2.16e-10
10	6.82e-14	1.13e-11	3.17e-11	1.82e-10	2.01e-10	4.29e-09	4.54e-09	5.28e-10	5.94e-09	–	4.46e-10
11	4.06e-13	5.02e-11	3.08e-10	1.46e-09	2.57e-09	5.11e-08	4.85e-08	4.47e-09	4.51e-08	2.86e-08	–

Table 4. Rate coefficients in units $cm^3\ s^{-1}$ for temperature $T = 6000$ K.

	1	2	3	4	5	6	7	8	9	10	11
1	–	1.59e-13	2.51e-14	7.88e-16	6.04e-16	9.84e-17	4.75e-17	9.09e-17	4.91e-17	5.61e-17	1.17e-17
2	6.78e-13	–	1.19e-10	1.50e-12	9.29e-13	1.08e-13	5.04e-14	6.43e-14	2.86e-14	2.75e-14	5.71e-15
3	2.20e-13	2.44e-10	–	9.16e-12	3.07e-12	4.49e-13	1.80e-13	2.14e-13	7.06e-14	1.14e-13	7.32e-14
4	2.97e-14	1.32e-11	3.94e-11	–	2.38e-10	1.67e-11	4.36e-12	3.81e-12	1.69e-12	2.55e-12	1.54e-12
5	5.84e-14	2.11e-11	3.39e-11	6.11e-10	–	6.17e-11	1.63e-11	9.78e-12	3.82e-12	7.21e-12	7.12e-12
6	6.32e-14	1.62e-11	3.28e-11	2.85e-10	4.09e-10	–	1.31e-09	2.23e-10	3.19e-10	9.58e-10	9.07e-10
7	1.40e-13	3.48e-11	6.05e-11	3.41e-10	4.96e-10	6.03e-09	–	2.75e-10	1.69e-09	4.81e-09	3.74e-09
8	2.33e-14	3.86e-12	6.25e-12	2.59e-11	2.59e-11	8.89e-11	2.39e-11	–	4.93e-11	6.02e-11	2.95e-11
9	3.49e-14	4.77e-12	5.73e-12	3.19e-11	2.81e-11	3.54e-10	4.09e-10	1.37e-10	–	2.66e-09	8.38e-10
10	1.25e-13	1.44e-11	2.89e-11	1.51e-10	1.66e-10	3.33e-09	3.63e-09	5.24e-10	8.33e-09	–	1.67e-09
11	3.60e-13	4.14e-11	2.58e-10	1.26e-09	2.27e-09	4.37e-08	3.92e-08	3.57e-09	3.63e-08	2.32e-08	–

Table 5. Rate coefficients in units $cm^3\ s^{-1}$ for temperature $T = 10\,000$ K.

	1	2	3	4	5	6	7	8	9	10	11
1	–	1.30e-12	2.80e-13	2.36e-14	1.60e-14	2.17e-15	8.94e-16	3.77e-15	2.36e-15	3.21e-15	1.21e-15
2	1.29e-12	–	1.96e-10	5.88e-12	3.39e-12	3.98e-13	1.78e-13	4.63e-13	2.29e-13	2.83e-13	9.62e-14
3	3.49e-13	2.46e-10	–	2.84e-11	9.55e-12	1.41e-12	4.47e-13	8.72e-13	3.37e-13	5.42e-13	6.56e-13
4	1.09e-13	2.75e-11	1.06e-10	–	3.82e-10	3.60e-11	9.00e-12	1.36e-11	5.80e-12	8.82e-12	1.06e-11
5	1.60e-13	3.42e-11	7.67e-11	8.26e-10	–	1.24e-10	3.06e-11	3.02e-11	1.34e-11	2.22e-11	4.69e-11
6	6.78e-14	1.25e-11	3.53e-11	2.42e-10	3.85e-10	–	1.50e-09	3.57e-10	4.41e-10	1.10e-09	2.66e-09
7	1.08e-13	2.17e-11	4.33e-11	2.34e-10	3.69e-10	5.81e-09	–	3.36e-10	1.88e-09	4.66e-09	8.52e-09
8	3.11e-14	3.85e-12	5.77e-12	2.41e-11	2.48e-11	9.46e-11	2.29e-11	–	4.74e-11	6.16e-11	5.48e-11
9	5.04e-14	4.94e-12	5.78e-12	2.67e-11	2.85e-11	3.03e-10	3.33e-10	1.23e-10	–	3.82e-09	1.37e-09
10	2.11e-13	1.88e-11	2.86e-11	1.25e-10	1.46e-10	2.33e-09	2.54e-09	4.92e-10	1.17e-08	–	2.79e-09
11	5.96e-13	4.80e-11	2.60e-10	1.13e-09	2.31e-09	4.21e-08	3.49e-08	3.29e-09	3.18e-08	2.10e-08	–

2.3 Data on Ca + H and Ca^+ + H^- collisions

Partial cross-sections and rate coefficients $K_{if}(T)$ for the excitation, de-excitation, mutual neutralization, and ion-pair formation processes in Ca + H and Ca^+ + H^- collisions are calculated in this work for the collision energy up to 145 eV and for the temperature range $T = 1000$–$10\,000$ K for all transitions between the scattering channels listed in Table 1. As mentioned above, the dominant mechanism of the processes treated is associated with the long-range ionic–covalent interactions. Since the most-valuable probabilities correspond to transitions due to long-range radial non-adiabatic couplings within one molecular symmetry, and the fact that the ground Ca^+ + H^- ionic molecular state has the $^2\Sigma^+$ symmetry, so covalent molecular states of the same symmetry are taken into account, that is, 10 low-lying $^2\Sigma^+$ covalent states in addition to the ground ionic molecular state, see Table 1. The calculated data are published online as supplementary material to this paper. For the temperatures $T = 3000$, 6000, and 10 000 K the calculated rate coefficients are also presented in Tables 3, 4, and 5. For $T = 6000$ K the rate coefficients are shown in Fig. 2 in the form of graphical representation.

It is seen from Fig. 2 and Tables 3, 4, and 5 that the mutual neutralization processes (the initial channel $i = 11$ = *ionic*) have the largest rate coefficients. At the temperature $T = 6000$ K, the largest rates correspond to neutralization into the final channels with the following atomic states:

Ca($4s5s\ ^3S$) ($11 \rightarrow 6$ transition), the rate $4.37 \times 10^{-8}\ cm^3\ s^{-1}$,
Ca($4s5s\ ^1S$) ($11 \rightarrow 7$), the rate $3.92 \times 10^{-8}\ cm^3\ s^{-1}$,
Ca($4s5p\ ^3P$) ($11 \rightarrow 9$), the rate $3.63 \times 10^{-8}\ cm^3\ s^{-1}$,
Ca($4s5p\ ^1P$) ($11 \rightarrow 10$), the rate $2.32 \times 10^{-8}\ cm^3\ s^{-1}$.

One can see that the largest rate coefficients exceed the value $10^{-8}\ cm^3\ s^{-1}$.

Fig. 3 exhibits the distribution of mutual neutralization rate coefficients at $T = 6000$ K as a function of the final-state binding

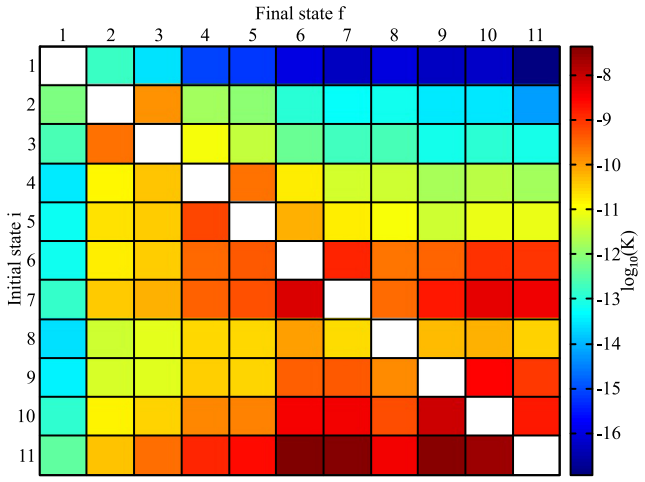

Figure 2. Graphical representation of the rate coefficients K_{if} (in units of $cm^3\ s^{-1}$) for the partial processes of excitation, de-excitation, mutual neutralization, and ion-pair formation at the temperature $T = 6000$ K. The channel numbers are collected in Table 1.

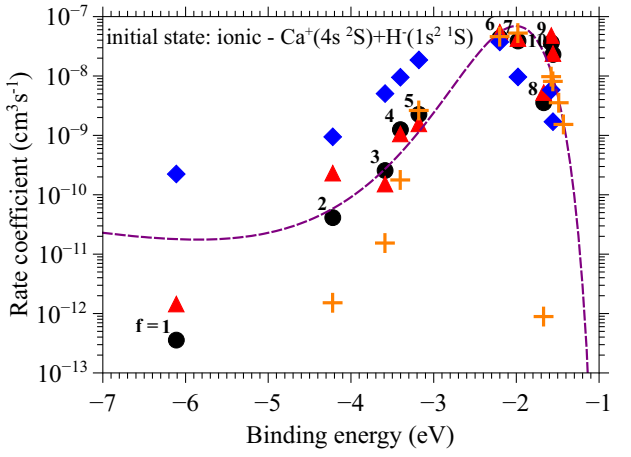

Figure 3. Distribution of the mutual neutralization rate coefficients $K_{if}(T)$ at $T = 6000$ K as a function of the final-state binding energy. The black circles correspond to the results of the present full quantum calculations, orange pluses to the calculations by the semi-empirical multichannel approach (Belyaev et al. 2016), the red triangles to the *ab initio* probability current method calculations (Belyaev et al. 2017), and the blue diamonds to the calculations by the LCAO multichannel approach (Barklem 2017). The dashed curve depicts the estimates from the simplified model (Belyaev & Yakovleva 2017).

energy. It is seen that in agreement with the prediction of the simplified model (Belyaev & Yakovleva 2017), the largest rate corresponds to neutralization into the final channel $f = 6$ from the optimal window, that is, the binding energy range in the vicinity of -2 eV. The processes into the final channels $f = 7$ and 9 have nearly the same rates as one into the final channel $f = 6$, since they are all belong to the optimal window. The neutralization rate into the final channel $f = 8$ is one order of magnitude smaller than the rates into the neighbouring channels because the molecular states $i = 11$ (*ionic*) and $f = 8$ are coupled by a two-electron-transition interaction while other ionic–covalent interactions are based on single-electron transitions. Outside of the optimal window in both directions, the rate coefficients decrease in agreement with the simplified model prediction although there are some deviations, the largest one is for the ground-state channel $f = 1$, otherwise the simplified model works surprisingly well.

The same Fig. 3 shows the results of other calculations (Belyaev et al. 2016, 2017; Barklem 2017) for these collisions, as well as the estimates from the simplified model (Belyaev & Yakovleva 2017). It is important to emphasize that the rate coefficients from Barklem (2017) are summed over all possible symmetries, while other results are the rates obtained in the $^2\Sigma^+$ symmetry only. It is seen that the probability current calculations (Belyaev et al. 2017) and the predictions from the simplified model agree well with the present full quantum calculations. The very good agreement is observed for the final channel $f = 6$ with the largest rate coefficient: All calculations give practically equal values within the uncertainty of 20–30 per cent. Outside of the optimal window, the deviations of the LCAO multichannel calculations from the full quantum one get more markable in both directions: underestimating for the higher lying final channels $f \geq 7$ and overestimating for the lower lying final channels $f \leq 5$. This is likely due to different electronic structures and the fact that the multichannel formulas account for the long-range non-adiabatic regions only, while both the full quantum (reprojection) method and the probability current method account for all long- and short-range regions.

Among the de-excitation processes in H-collisions, the largest rates at $T = 6000$ K correspond to the following processes:

$$Ca(4s5p\ ^1P) + H \rightarrow Ca(4s5p\ ^3P) + H,$$

the transition $10 \rightarrow 9$, the rate 8.33×10^{-9} $cm^3\ s^{-1}$, and

$$Ca(4s5s\ ^1S) + H \rightarrow Ca(4s5s\ ^3S) + H,$$

the transition $7 \rightarrow 6$, the rate 6.03×10^{-9} $cm^3\ s^{-1}$.

Among the excitation processes, the largest rate coefficients at $T = 6000$ K correspond to the following transitions:

$Ca(4s5s\ ^1S) + H \rightarrow Ca(4s5p\ ^1P) + H$, $(7 \rightarrow 10)$, the rate 4.81×10^{-9} $cm^3\ s^{-1}$,

$Ca(4s5p\ ^3P) + H \rightarrow Ca(4s5p\ ^1P) + H$, $(9 \rightarrow 10)$, the rate 2.66×10^{-9} $cm^3\ s^{-1}$.

It is seen that the maximal neutralization rate is at least 5 times larger than the largest (de)-excitation rates. The rate coefficients for other processes have typically values between 10^{-17} and 10^{-9} $cm^3\ s^{-1}$.

According to the simplified model (Belyaev & Yakovleva 2017), the distribution of the inelastic rate coefficients for excitation and de-excitation processes depends on both initial and final state binding energies. For this reason, Figs 4, 5, and 6 show the distributions of the rate coefficients for the different initial channels i, namely, for $i = 10$, 9, and 7, respectively. Indeed, one can see that the distributions for the different initial channels and, hence, for the different initial channel binding energies are different. In addition, one can see a scatter of the data calculated by different methods, a greater scatter for (de)-excitation than for the mutual neutralization processes. One can conclude that the prediction of the simplified model gives a good order of magnitude for the mutual-neutralization/ion-pair-formation rate coefficients as long as long-range ionic–covalent interactions are dominant, while the agreement is less satisfactory for excitation/de-excitation.

Temperature dependences of the large-valued rate coefficients of mutual neutralization processes are shown in Fig. 7. The data from the full quantum calculations (solid lines) are compared with the probability current method results (symbols). First of all, it can be seen in this figure that the neutralization rates are weakly varying with the temperature. The same conclusion holds for the de-

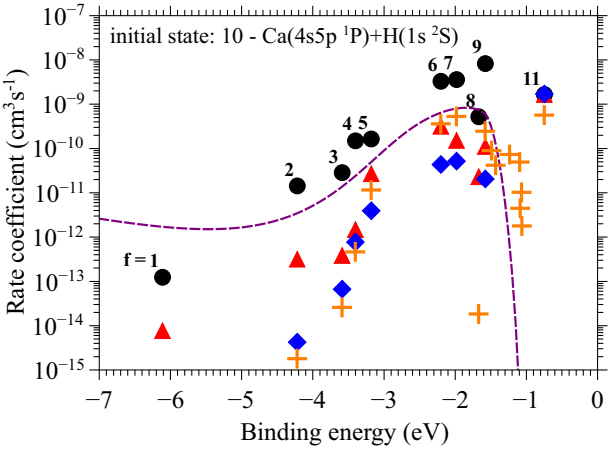

Figure 4. De-excitation ($f \leq 9$) and ion-pair formation ($f = 11$) rate coefficients $K_{if}(T)$ at $T = 6000$ K for the initial channel $i = 10$ as functions of the final-state binding energy. The key legends are given in Fig. 3.

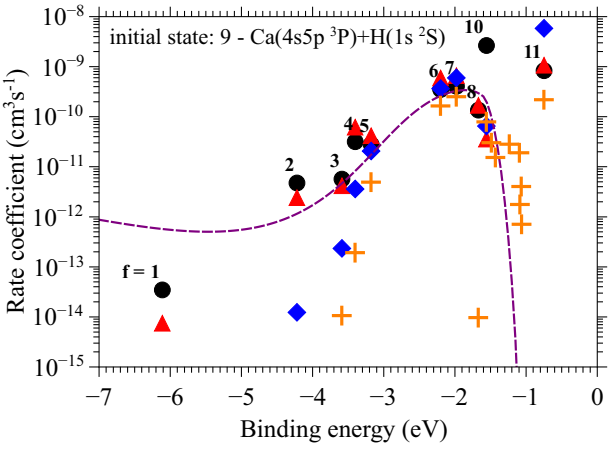

Figure 5. De-excitation ($f \leq 8$), excitation ($f = 10$), and ion-pair formation ($f = 11$) rate coefficients $K_{if}(T)$ at $T = 6000$ K for the initial channel $i = 9$ as functions of the final-state binding energy. The key legends are given in Fig. 3.

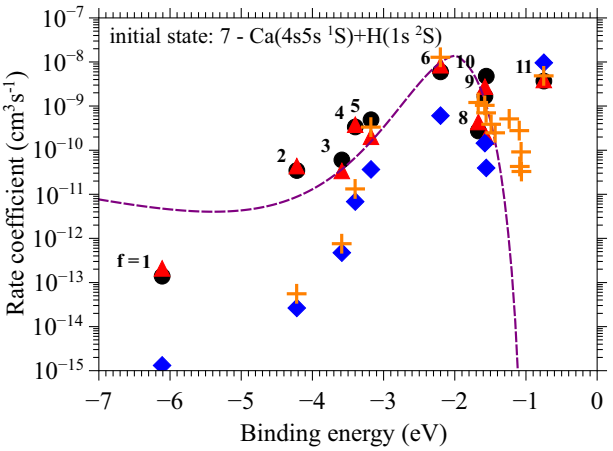

Figure 6. De-excitation ($f \leq 6$), excitation ($f = 8$–10), and ion-pair formation ($f = 11$) rate coefficients $K_{if}(T)$ at $T = 6000$ K for the initial channel $i = 7$ as functions of the final-state binding energy. The key legends are given in Fig. 3.

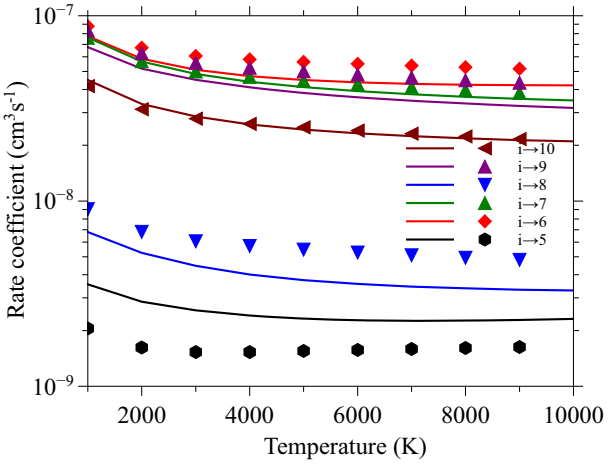

Figure 7. Temperature dependence of the mutual neutralization rate coefficients for the transitions $i = 11$ (*ionic*) $\rightarrow f = 10, 9, 8, 7, 6, 5$ calculated by the full quantum approach (solid lines) and by the probability current method (symbols).

excitation processes. Second, one can see that both methods provide close results over the whole temperature range treated. This helps to determine reaction mechanisms.

The analysis of the nuclear dynamics shows that the inelastic processes with the large-valued rate coefficients occur due to long-range ionic–covalent interactions, when covalent states are located in the optimal window. The examples are the mutual neutralization processes $11 \rightarrow 6$, $11 \rightarrow 7$, $11 \rightarrow 9$, and $11 \rightarrow 10$, as well as the (de)-excitation processes $10 \rightarrow 9$, $7 \rightarrow 6$, $7 \rightarrow 10$, and $9 \rightarrow 10$, etc. For many processes with low- and moderate-valued rates, short-range non-adiabatic regions contribute significantly into inelastic transitions in addition to the long-range non-adiabatic regions. In these cases, the reaction mechanism is due to several non-adiabatic regions, both long and short ranges.

3 CONCLUSIONS

The present full quantum study of the inelastic processes in Ca + H and Ca^+ + H^- collisions is based on the accurate *ab initio* adiabatic potentials and non-adiabatic couplings calculated by Mitrushchenkov et al. (2017). It has been shown by the model studies that the dominant non-adiabatic transitions in calcium–hydrogen collisions occur within the CaH($^2\Sigma^+$) molecular symmetry, so only this symmetry is included into the present quantum study. The ground ionic $Ca^+ + H^-$ state and 10 low-lying covalent molecular states of the $^2\Sigma^+$ symmetry are included into the present CaH nuclear dynamic treatment. The non-adiabatic nuclear dynamics is studied by means of the reprojection method (Grosser et al. 1999; Belyaev et al. 2001; Belyaev 2010).

The *ab initio* electronic structure exhibits the presence of several narrow non-adiabatic regions, which cause the problems for numerical integration of the coupled channel equations for radial nuclear wave functions. In order to solve these problems, the quantum chemical data are transferred from the adiabatic to the hybrid diabatic representation. The hybrid diabatization method (Vlasov et al. 2018) is applied only into narrow non-adiabatic regions. The non-adiabatic nuclear dynamics is then treated in the hybrid diabatic representation. Since the obtained hybrid representation coincides with the adiabatic one in the asymptotic region, the asymptotic non-adiabatic couplings remain non-zero, and these non-zero couplings

are taken into account by the reprojection method for calculating the scattering matrix.

The present accurate full quantum treatment shows that the largest rate coefficients correspond to the mutual neutralization processes with the final-channel energies from the optimal window, that is, when the final-channel binding energies are around −2 eV. The largest neutralization rates have the values exceeding 10^{-8} cm^3 s^{-1}. The reaction mechanism for these processes is based on the long-range ionic–covalent interactions. Among de-excitation and excitation processes, the maximal rate coefficients at least 5 times smaller than the maximal neutralization rate and correspond to the de-excitation transitions Ca($4s5p\,^1P$) → Ca($4s5p\,^3P$) and Ca($4s5s\,^1S$) → Ca($4s5s\,^3S$) induced by H-collisions. These transitions correspond to the spin-forbidden atomic transitions between singlet and triplet states. But non-adiabatic transitions in collisions occur between molecular states and, hence, the atomic selection rules are not valid any more. The collisional processes with moderate and low values of the rate coefficients are based on non-adiabatic transitions which are located in both long- and short-range non-adiabatic regions. Therefore, omitting short-range regions might underestimate rate coefficients.

The calculated collision data are compared with other available data, which were obtained by the model approaches. The very good agreement is found for the processes with the large-valued rate coefficients. For the processes with moderate and low values of the rate coefficients some deviations are observed. The better agreement is found for the rates computed by the probability current method, which accounts not only long-range non-adiabatic regions, but also short-range regions. The calculated data are available online.

ACKNOWLEDGEMENTS

AKB and DVV gratefully acknowledge support from the Russian Science Foundation (grant number 17-13-01144). The authors also gratefully acknowledge Paris–Meudon Observatory for partial support and Dr. Christian Balanca for fruitful discussions.

REFERENCES

Asplund M., 2005, ARA&A, 43, 481
Barklem P. S., 2016a, A&AR, 24, 1
Barklem P. S., 2016b, Phys. Rev. A, 93, 042705
Barklem P. S., 2017, Phys. Rev. A, 95, 069906
Barklem P. S., Belyaev A. K., Guitou M., Feautrier N., Gadéa F. X., Spielfiedel A., 2011, A&A, 530, A94
Belyaev A. K., 1993, Phys. Rev. A, 48, 4299
Belyaev A. K., 2010, Phys. Rev. A, 82, 060701
Belyaev A. K., 2013, Phys. Rev. A, 88, 052704
Belyaev A. K., Barklem P. S., 2003, Phys. Rev. A, 68, 062703
Belyaev A. K., Yakovleva S. A., 2017, A&A, 606, A147
Belyaev A. K., Grosser J., Hahne J., Menzel T., 1999, Phys. Rev. A, 60, 2151
Belyaev A. K., Egorova D., Grosser J., Menzel T., 2001, Phys. Rev. A, 64, 052701
Belyaev A. K., Barklem P. S., Dickinson A. S., Gadéa F. X., 2010, Phys. Rev. A, 81, 032706
Belyaev A. K., Barklem P. S., Spielfiedel A., Guitou M., Feautrier N., Rodionov D. S., Vlasov D. V., 2012, Phys. Rev. A, 85, 032704
Belyaev A. K., Yakovleva S. A., Guitou M., Mitrushchenkov A. O., Spielfiedel A., Feautrier N., 2016, A&A, 587, A114
Belyaev A. K., Voronov Y. V., Yakovleva S. A., Mitrushchenkov A., Guitou M., Feautrier N., 2017, ApJ, 851, 59
Belyaev A. K., Voronov Y. V., Gadéa F. X., 2018, ApJ, 867, 87
Caffau E. et al., 2011, Nature, 477, 67
Christlieb N. et al., 2002, Nature, 419, 904
Cohen J. G., Christlieb N., Thompson I., McWilliam A., Shectman S., Reimers D., Wisotzki L., Kirby E., 2013, ApJ, 778, 56
Croft H., Dickinson A. S., Gadéa F. X., 1999a, J. Phys. B: At. Mol. Opt. Phys., 32, 81
Croft H., Dickinson A. S., Gadéa F. X., 1999b, MNRAS, 304, 327
Drake J. J., 1991, MNRAS, 251, 369
Drawin H.-W., 1968, Z. Phys., 211, 404
Drawin H.-W., 1969, Z. Phys., 225, 483
Frebel A. et al., 2005, Nature, 434, 871
Frebel A., Chiti A., Ji A. P., Jacobson H. R., Placco V. M., 2015, ApJ, 810, L27
Grosser J., Menzel T., Belyaev A. K., 1999, Phys. Rev. A, 59, 1309
Guitou M., Spielfiedel A., Rodionov D. S., Yakovleva S. A., Belyaev A. K., Merle T., Thévenin F., Feautrier N., 2015, Chem. Phys., 462, 94
Idiart T., Thevenin F., 2000, ApJ, 541, 207
Lambert D. L., 1993, Phys. Scr., T47, 186
Landau L., 1932a, Phys. Z. Sowjet., 1, 88
Landau L., 1932b, Phys. Z. Sowjet., 2, 46
Mashonkina L., Korn A. J., Przybilla N., 2007, A&A, 461, 261
Mashonkina L. I., Sitnova T. N., Pakhomov Y. V., 2016, Astron. Lett., 42, 606
Mashonkina L., Sitnova T., Belyaev A. K., 2017, A&A, 605, A53
Mitrushchenkov A., Guitou M., Belyaev A. K., Yakovleva S. A., Spielfiedel A., Feautrier N., 2017, J. Chem. Phys., 146, 014304
Mitrushenkov A. O., Palmieri P., Puzzarini C., Tarroni R., 2000, Mol. Phys., 98, 1677
Norris J. E., Christlieb N., Korn A. J., Eriksson K., Bessell M. S., Beers T. C., Wisotzki L., Reimers D., 2007, ApJ, 670, 774
Plaskett H. H., 1955, MNRAS, 115, 256
Roos J. B., Orel A. E., Larson Å., 2009a, Phys. Rev. A, 79, 062510
Roos J. B., Larsson M., Larson Å., Orel A. E., 2009b, Phys. Rev. A, 80, 012501
Sitnova T. M., Mashonkina L. I., Ryabchikova T. A., 2018, MNRAS, 477, 3343
Steenbock W., Holweger H., 1984, A&A, 130, 319
Stenrup M., Larson Å., Elander N., 2009, Phys. Rev. A, 79, 012713
Vlasov D. V., Rodionov D. S., Belyaev A. K., 2018, Opt. Spectrosc., 124, 611
Voorhis T. V., Kowalczyk T., Kaduk B., Wang L.-P., Cheng C.-L., Wu Q., 2010, Annu. Rev. Phys. Chem., 61, 149
Yakovleva S. A., Voronov Y. V., Belyaev A. K., 2016, A&A, 593, A27
Zanchet A., Bañares L., Senent M. L., García-Vela A., 2016, Phys. Chem. Chem. Phys., 18, 33195
Zener C., 1932, Proc. R. Soc. A, 137, 696

SUPPORTING INFORMATION

Supplementary data are available at *MNRAS* online.

Supplementary data are presented in the files **ReadMe.txt, rc1000.dat, rc2000.dat, rc3000.dat, rc4000.dat, rc5000.dat, rc6000.dat, rc7000.dat, rc8000.dat, rc9000.dat, rc10000.dat**. The files *.dat contain rate coefficients in units of cm^3 s^{-1} for inelastic Ca + H and Ca$^+$ + H$^-$ collisions for temperatures from T = 1000 K to T = 10 000 K.

Please note: Oxford University Press is not responsible for the content or functionality of any supporting materials supplied by the authors. Any queries (other than missing material) should be directed to the corresponding author for the article.

This paper has been typeset from a TEX/LATEX file prepared by the author.